PHYSICAL REVIEW B **89**, 081107(R) (2014)

Typical medium dynamical cluster approximation for the study of Anderson localization in three dimensions

C. E. Ekuma,[1,2,*] H. Terletska,[1,3] K.-M. Tam,[1,2] Z.-Y. Meng,[1,2,4] J. Moreno,[1,2] and M. Jarrell[1,2,†]

[1]*Department of Physics & Astronomy, Louisiana State University, Baton Rouge, Louisiana 70803, USA*

[2]*Center for Computation and Technology, Louisiana State University, Baton Rouge, Louisiana 70803, USA*

[3]*Brookhaven National Laboratory, Upton, New York 11973, USA*

[4]*Department of Physics, University of Toronto, Toronto, Ontario M5S 1A7, Canada*

(Received 17 September 2013; revised manuscript received 13 November 2013; published 14 February 2014)

We develop a systematic typical medium dynamical cluster approximation that provides a proper description of the Anderson localization transition in three dimensions (3D). Our method successfully captures the localization phenomenon both in the low and large disorder regimes, and allows us to study the localization in different momenta cells, which renders the discovery that the Anderson localization transition occurs in a cell-selective fashion. As a function of cluster size, our method systematically recovers the reentrance behavior of the mobility edge and obtains the correct critical disorder strength for Anderson localization in 3D.

DOI: 10.1103/PhysRevB.89.081107 PACS number(s): 72.15.Rn, 02.70.Uu, 64.70.Tg, 72.80.Ng

Introduction. The search for new methods to better understand Anderson localization [1,2] remains an active area in the study of disordered electronic systems [3]. Here, the scattering of charge carriers off random impurities [4,5] may inhibit their propagation across the sample leading to a phenomenon known as Anderson localization [1]. Despite intensive studies, a proper mean-field theory of this phenomenon remains elusive.

The most commonly used mean-field theory to study disordered systems is the coherent potential approximation (CPA) [6,7], where the original disordered lattice is replaced by an impurity embedded in an effective medium. The CPA successfully describes some one-particle properties, such as the density of states (DOS) in substitutional disordered alloys [6,7], but fails to capture the Anderson localization transition (ALT). As a local approximation, the CPA is unable to capture crucial multiple backscattering interference effects that can lead to localization. Cluster extensions of the CPA such as the dynamical cluster approximation (DCA) [8,9] and the molecular CPA [10] incorporate nonlocal effects; however, they still fail to describe the ALT. The average DOS calculated within such mean-field theories cannot distinguish between extended and localized states and it is not critical at the transition [9]; hence, it cannot be used as an order parameter. Finding a proper single-particle order parameter for the ALT capable of distinguishing between localized and extended states is a major challenge in the study of disordered electronic systems.

While at the ALT the average DOS is not critical [11], the geometrical mean of the local DOS (LDOS) [12–15], which better approximates the typical value of the LDOS, is actually critical. Dobrosavljević *et al*. [16] incorporated such geometric averaging over disorder in the typical medium theory (TMT) where the typical and not the average LDOS is used in the CPA self-consistency loop. They showed that the typical DOS (TDOS) obtained from geometric averaging over disorder becomes critical at the transition, and hence can serve as an appropriate order parameter for the ALT.

The local TMT reproduces some of the expected features of the ALT, but fails to provide a proper description of the critical behavior in three dimensions (3D). It underestimates the critical disorder strength with $W_c^{\mathrm{TMT}} \approx 1.65$ instead of the numerical value $W_c \approx 2.1$ [17–20] (in a unit where $4t = 1$), and the critical exponent of the order parameter $\beta^{\mathrm{TMT}} \approx 1.0$, whereas the recently reported value is $\beta \approx 1.67$ [20,21]. Another crucial drawback of the local TMT in 3D is that it cannot describe the reentrant behavior of the mobility edge (the energy separating extended and localized electron states) as seen in transfer matrix method studies [4,22]. Hence, by its construction the TMT is able to describe the effects of strong localization due to disorder, but all nonlocal spatial correlation effects are missed [23].

A natural way to improve upon the local TMT is to construct its cluster extension using the DCA scheme, which systematically incorporates nonlocal effects. Recently, we extended the local TMT to a cluster version called the cluster typical medium theory (CTMT) [24]. Here, the diagonal cluster-momentum-resolved density of states is replaced by its typical value $\rho^c(K,\omega) = \exp(\langle \ln\, \rho^c(K,\omega)\rangle)$. This scheme works well in lower dimensions, where weak localization effects are most pronounced, and our results reveal that all the states are localized in the large cluster limit. However, this formalism does not properly describe the ALT in a 3D lattice. The reason is that in 3D, at a given disorder strength below the critical value W_c, there are regions of the DOS consisting of only localized states, and others only extended states. To capture this mixing of localized and extended states requires that different energy scales are treated separately. Our CTMT formalism fails in 3D because the DOS at each cluster site is first averaged over the cluster to obtain $\rho^c(K,\omega)$. For large clusters, it will not contain any information about the localization edge, and a theory based upon it is unable to distinguish between states above and below the localization edge.

In this Rapid Communication, to avoid such self-averaging issues in the TDOS, we propose a different typical medium DCA (TMDCA) method by explicitly separating out the local part of the TDOS and treating it with a geometric averaging over disorder configurations. In this way, we are able to obtain a proper TDOS that characterizes the ALT in 3D. The method

*cekuma1@lsu.edu

†jarrellphysics@gmail.com

we develop is a systematic self-consistent effective medium theory to study ALT in 3D, which (i) recovers the original local TMT scheme at $N_c = 1$; (ii) recovers the DCA for small W (when all states are metallic); (iii) provides a proper way to *treat the different energy scales* such that the *characteristic reentrant behavior of the mobility edge* is obtained; (iv) captures the critical behavior of the ALT with *correct critical disorder strength*; (v) provides a correct description of the Anderson insulator at large W when all states are localized; and (vi) fulfills all *the essential requirements expected of a "successful" cluster theory* [9,25] including causality and translational invariance.

Method. We consider the Anderson model of noninteracting electrons subjected to a random potential. The Hamiltonian is given by

$$H = -\sum_{\langle ij\rangle} t_{ij}(c_i^\dagger c_j + \text{H.c.}) + \sum_i V_i n_i. \tag{1}$$

The disorder is modeled by a local potential V_i randomly distributed according to a probability distribution $P(V_i)$. The operator $c_i^\dagger$ (c_i) creates (annihilates) an electron on site i, $n_i = c_i^\dagger c_i$ is the number operator, and t_{ij} is the hopping matrix element between nearest-neighbor (NN) sites $\langle i,j\rangle$. We set $4t = 1$ as the energy unit, and use a "box" distribution with $P(V_i) = \frac{1}{2W}\Theta(W - |V_i|)$, where $\Theta(x)$ is a step function. We use the shorthand notation $\langle\cdots\rangle = \int dV_i P(V_i)(\cdots)$ for disorder averaging.

To solve the Hamiltonian (1) we utilize a modification of the standard DCA procedure [9]. Here, the original lattice model is mapped onto a periodic cluster of size $N_c = L_c^3$ embedded in a self-consistent typical medium characterized by a nonlocal hybridization function $\Gamma(K,\omega)$. Hence, spatial correlations up to a range $\xi \lesssim L_c$ are treated explicitly, while the longer length scale physics is described at the mean-field level. The mapping is accomplished by dividing the first Brillouin zone into N_c nonoverlapping cells of equal size. The lattice Green function is coarse-grained over the cells, and the cluster self-energy is subtracted to form the cluster-excluded Green function $\mathcal{G}(K,\omega) = [\omega - \Gamma(K,\omega) - \bar{\epsilon}_K]^{-1}$, where $\bar{\epsilon}_K$ is the coarse-grained bare dispersion. $\mathcal{G}(K,\omega)$ is Fourier transformed to form the real space $\mathcal{G}_{n,m} = \sum_K \mathcal{G}(K)\exp[iK\cdot(r_n - r_m)]$. Then for each randomly chosen disorder configuration V, we calculate the cluster Green function $G^c(V) = (\mathcal{G}^{-1} - V)^{-1}$.

From this quantity we obtain the typical density of states $\rho^c_{typ}(K,\omega)$ which is constructed as

$$\rho^c_{typ}(K,\omega) = \overbrace{\exp\left(\frac{1}{N_c}\sum_{i=1}^{N_c}\left\langle \ln \rho_i^c(\omega,V)\right\rangle\right)}^{\text{local TDOS}} \underbrace{\left\langle \frac{\rho^c(K,\omega,V)}{\frac{1}{N_c}\sum_i \rho_i^c(\omega,V)}\right\rangle}_{\text{nonlocal}}. \tag{2}$$

Here, $\rho_i^c(\omega,V) = -\frac{1}{\pi}\text{Im}\, G_{ii}^c(\omega,V)$, while $\rho^c(K,\omega,V) = -\frac{1}{\pi}\text{Im}\, G^c(K,\omega,V)$ is obtained from the diagonal Fourier transform of the cluster Green function $G_{ij}^c(\omega,V)$.

As mentioned in the Introduction, to avoid self-averaging as N_c increases, we modify our CTMT [24] scheme in the way we calculate the spectra $\rho^c_{typ}(K,\omega)$ used in the self-consistency. In particular, as shown in Eq. (2), we separate the "local TDOS," and treat it with geometrical averaging over disorder, from the "nonlocal" part which is treated via algebraic averaging.

This $\rho^c_{typ}(K,\omega)$ possesses the following properties: for $N_c = 1$, it reduces to the local TMT with $\rho^c_{typ}(\omega) = \exp\langle\ln\rho^c(\omega,V)\rangle$. At low disorder strength $W \ll W_c$ the local real space prefactor $\langle\ln\rho_i^c(\omega,V)\rangle \approx \ln\langle\rho_i^c(\omega,V)\rangle$. Then $\rho^c_{typ}(K,\omega)$ reduces to the DOS calculated in DCA scheme, with $\rho^c_{typ}(K,\omega) \to \langle\rho^c(K,\omega,V)\rangle$.

From Eq. (2), the disorder averaged typical cluster Green function is obtained using the Hilbert transform $G^c_{typ}(K,\omega) = \int d\omega' \frac{\rho^c_{typ}(K,\omega')}{\omega-\omega'}$. Finally, the self-consistency loop is closed by calculating the coarse-grained cluster Green function of the lattice

$$\overline{G}(K,\omega) = \int \frac{N_0^c(K,\epsilon)d\epsilon}{\left[G^c_{typ}(K,\omega)\right]^{-1} + \Gamma(K,\omega) - \epsilon + \bar{\epsilon}(K) + \mu},$$

where $N_0^c(K,\epsilon)$ is the bare partial density of states.

We note that our formalism preserves causality just as the DCA [9], since all the Green functions are causal, both the DOS and the TDOS calculated from them are positive definite. Also, we observe that as N_c increases, our method systematically interpolates between the local TMT and the exact result.

Results and Discussion. We start the discussion of our results by comparing the algebraically averaged DOS (ADOS) and the TDOS for $N_c = 1$ and 38 at various disorder strengths (Fig. 1). Our TMDCA scheme for $N_c = 1$ corresponds to the original TMT procedure. The ADOS is obtained from the

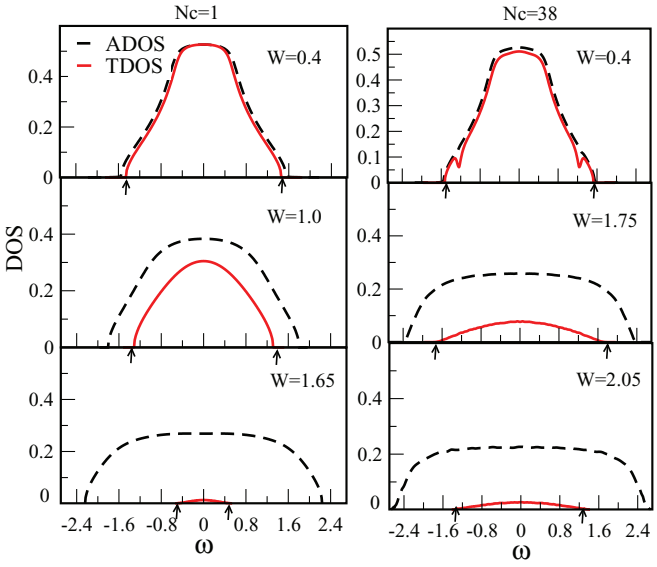

FIG. 1. (Color online) Evolution of the ADOS and TDOS at different disorder strength W for the TMT ($N_c = 1$) and TMDCA with $N_c = 38$. At low disorder, where all the states are metallic, the TDOS is the same as the ADOS. As W increases the TDOS gets suppressed. In the local TMT, the mobility edge (indicated by arrows) moves towards $\omega = 0$ monotonically. In the TMDCA the mobility edge first moves to higher energy, and around $W > 1.75$ it starts moving towards the band center, indicating that TMDCA can successfully capture the reentrance behavior missing in the TMT scheme.

conventional DCA scheme, where the ADOS is used in the self-consistency. As can be seen from Fig. 1 for both TMT ($N_c = 1$) and TMDCA ($N_c = 38$), the ADOS remains finite while the TDOS gets suppressed as W_c is approached.

Hence, the TDOS indeed serves as a proper order parameter of the ALT. In addition, at low disorder, $W = 0.4$, for $N_c = 38$, the ADOS and TDOS are practically the same, indicating that our TMDCA procedure at $W \ll W_c$ reduces to the DCA scheme in agreement with our analytical analysis described above. Moreover, a crucial difference between the local TMT at $N_c = 1$ and TMDCA at $N_c = 38$ can be seen from the comparison of the left and right panels of Fig. 1. The mobility edge, separating extended from localized states, is defined by the boundary of the TDOS and indicated by arrows. For the local TMT the edge always gets narrower with increasing W, while for TMDCA, the mobility edge first expands and then retracts, hence giving rise to the reentrance behavior, which is missed in the local TMT.

Next, we consider the evolution of W_c with N_c. Figure 2 shows the TDOS at the band center as a function of W for several N_c. W_c is defined by the vanishing of the TDOS ($\omega = 0$). Our results show that as cluster size N_c increases, for $N_c \geqslant 12$ the W_c systematically increases until it converges to $W_c \approx 2.1$ (for details, see Supplemental Material (SM) [26]) which is in good agreement with the values reported in the literature [4,17,18,20–22,27]. This cluster is the first one with a complete NN shell (for details, see SM [26]). From this cluster onward, W_c converges to ≈ 2.1. Fitting the data for the two largest clusters starting from $W \approx 1.0$ with a power law TDOS $(\omega = 0) = a_0|W - C|^{\beta}$, we obtain $\beta > 1.40$, which is greater than a single site TMT value of $\beta^{TMT} = 1.0$; but it is still smaller than the most recently reported $\beta \approx 1.67$ [20,21,28]. We note that other mean-field methods reported $\beta \lesssim 1.0$ [29]. In our method, we note that it is unlikely that we can calculate the critical disorder strength and exponents as precisely as diagonalization and transfer matrix methods [4,17,18,20–22,27]. However, the advantage of our method is that we can incorporate both interactions and realistic electronic structure as in, e.g., the dynamical mean-field theory [30] and other DCA calculations (see, e.g., Ref. [31]).

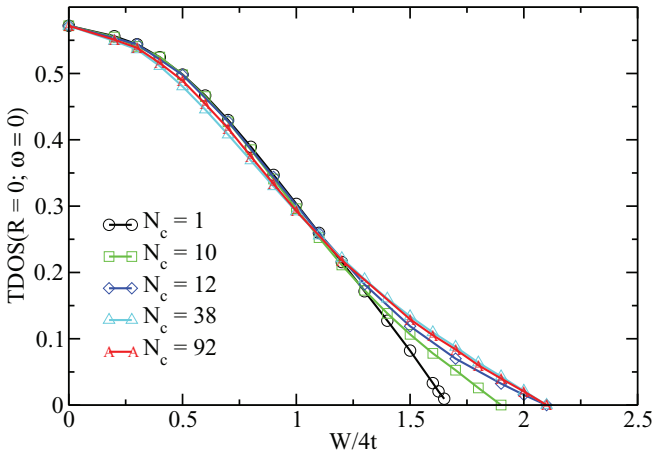

FIG. 2. (Color online) The TDOS ($\omega = 0$) vs W for different cluster sizes $N_c = 1,10,12,38,92$. The TDOS ($\omega = 0$) vanishes at W_c where all states become localized. For $N_c = 1$ (TMT), the critical disorder strength $W_c^{N_c=1} \approx 1.65$. As N_c increases, W_c increases quickly to $W_c^{N_c \geqslant 12} \approx 2.10 \pm 0.01$.

The probability distribution function (PDF) is a natural way to characterize the 3D Anderson localization transition. This is due to the fact that the "typical" value of a "random" variable corresponds to the most probable value of the PDF [21,24].

Since, for a proper description of electron localization in disordered systems, one should focus on the distribution functions of the quantities of interest [1], we calculate the PDF of the cluster-momentum-resolved DOS $\rho(K,\omega = \bar{\epsilon}_K)$ (at different momenta cells K and energy $\omega = \bar{\epsilon}_K$) sampled over a large number of disorder configurations. Our results for the evolution of the PDF$[\rho(K,\omega = \bar{\epsilon}_K)]$ with W are shown in Fig. 3.

From statistical studies of disordered systems [12,22], it is known that for extended states, when the amplitude of the wave function is approximately the same on every site, the distribution of the local DOS is Gaussian and the most probable value coincides with the arithmetic mean. On the other hand, for localized states, which have substantial weight on a few sites only, the distributions develop long tails and are extremely asymmetric with a log-normal shape. Most of the weight is concentrated around zero, and its most probable value is much smaller than the arithmetic mean. As can be seen from Fig. 3, we indeed observe such behavior in our results. In particular, we find that as W increases, different cluster cells localize at different rates. The cells centered at cluster momenta $K = (0,0,0)$ and (π,π,π) (labeled as D in Fig. 3) and energy at the band edges have the same PDF. They

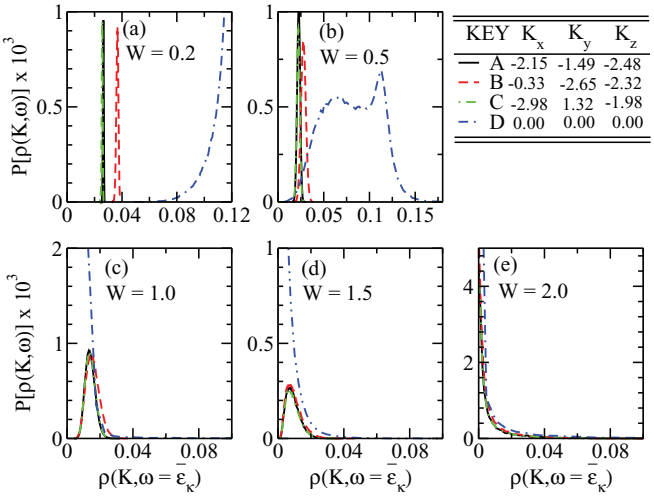

FIG. 3. (Color online) The evolution of the probability distribution of the cluster-momentum-resolved DOS at different cluster cells, PDF$[\rho(K,\omega = \bar{\epsilon}_K)]$, with increasing W for $N_c = 38$. The labels A–D and their associated momenta K correspond to each of the four distinct cells obtained using the point-group and particle-hole symmetry $[\rho(K,\omega) = \rho(Q - K, -\omega)$, with $Q = (\pi,\pi,\pi)]$ of the cluster. Before the localization transition, the edge cells [corresponding to (0,0,0) and (π,π,π) label D] develop a log-normal distribution while other cells remain Gaussian at small and moderate W [(a)–(d)]. Close to the critical disorder strength $W = 2.0$, panel (e), all the cells show log-normal distributions.

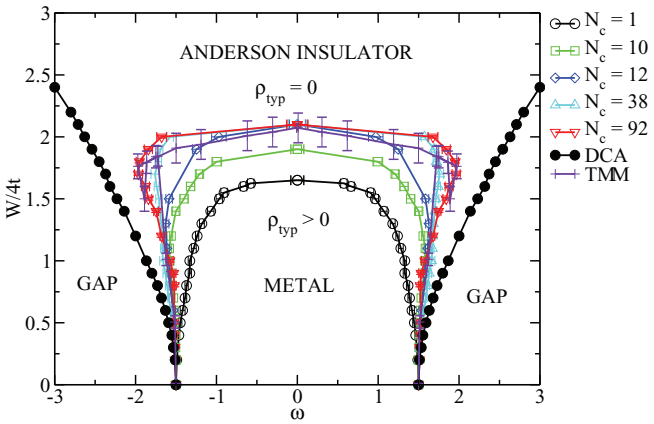

FIG. 4. (Color online) Phase diagram of the Anderson localization transition in 3D obtained from TMDCA simulations. As N_c increases, a systematic improvement of the trajectory of the mobility edge is achieved. At large enough N_c and within computation error, our results converge to those determined by the TMM [4].

localize much faster than other cells with lower energies. The PDFs of these edge cells exhibit log-normal distribution far earlier than other cells which remain Gaussian up to moderate disorder strengths $W \sim 1.0$ [panel (c)]. However, close to W_c [cf. Fig. 3(e)], all the cells show log-normal distributions with their most probable values peaked close to zero. For $W = W_c$ all the states are localized and the system undergoes a full ALT in agreement with numerically exact results [32]. Hence, the localization transition occurs as a "*momentum cell-selective Anderson localization transition*."

Finally, in Fig. 4 we present the phase diagram in the disorder-energy (W-ω) plane for the 3D ALT constructed from our TMDCA procedure. Here, we show the mobility edge trajectories given by the frequencies where the TDOS vanishes at a given disorder strength W, and the band edge determined by the vanishing of the ADOS calculated within the DCA. For comparison, we also present the numerical results from the transfer matrix method in Ref. [4]. For large enough clusters, $N_c = 92$, our results converge to their results within the errors of both approaches. In particular, as N_c increases, the mobility edge trajectories are systematically reproduced, with reentrance behavior gradually captured.

As evident from Fig. 4, at $N_c = 12$ (the first cluster with complete NN shell), the W_c at $\omega = 0$ quickly converges to $W_c = 2.1$, while the trajectory of the mobility edge continues to change with N_c. This may be understood from the different localization mechanisms for states at the band center and edge [4]. States at the band center become localized mainly due to coherent backscattering, while those above and below the bare band edges are initially localized in deeply trapped states. They become delocalized with increasing W due to the increasing DOS and hence increasing quantum tunneling between the deeply trapped states. They finally become localized again with increasing disorder, which explains the reentrant behavior. Since coherent backscattering requires a retracing of the electronic path, the effective length scales captured by the cluster are doubled, so W_c converges very quickly at the band center. On the other hand, the quantum tunneling mechanism has no path doubling and requires multiple deeply trapped states on the cluster and therefore converges more slowly with N_c.

Conclusions. In this Rapid Communication we develop a DCA-based typical medium theory (TMDCA) to study Anderson localization in three dimensions. The developed TMDCA presents a successful self-consistent, causal, and numerically manageable effective medium scheme of Anderson localization. Employing the one-particle typical density of states as an order parameter of the Anderson transition, the TMDCA gives the critical disorder strength of $W_c = 2.10 \pm 0.01$ which is in very good agreement with the acceptable value in literature, and it is of noticable improvement over the single-site TMT result of $W_c = 1.65$. Moreover, our method systematically captures the reentrance behavior of the mobility edge trajectories, which are absent in the local TMT scheme. Our analyses further show *a cell-selective Anderson localization transition*, with different cluster cells localizing at different rates. Our TMDCA method is easy to implement and computationally inexpensive since it requires only the computer time required to diagonalize small clusters, average over the disorder, and iterate to convergence. Once combined with electronic structure calculations [33] and more sophisticated many-body techniques for electron interactions, it will open a new avenue for studying localization phenomenon in real materials as well as the competition between disorder and electron correlations.

Acknowledgments. We thank V. Dobrosavljević, S.-X. Yang, and C. Moore for useful discussions. This work is supported by the DOE BES CMCSN Grant No. DE-AC02-98CH10886 (H.T.) and SciDAC Grant No. DE-SC0005274 (M.J. and K.M.T), and the NSF EPSCoR Cooperative Agreement No. EPS-1003897 (C.E., Z.Y.M., and J.M.). Supercomputer support is provided by the Louisiana Optical Network Initiative (LONI) and HPC@LSU computing resources.

[1] P. W. Anderson, Phys. Rev. **109**, 1492 (1958).

[2] E. Abrahams, P. W. Anderson, D. C. Licciardello, and T. V. Ramakrishnan, Phys. Rev. Lett. **42**, 673 (1979).

[3] *50 Years of Anderson Localization*, edited by E. Abrahams (World Scientific, Singapore, 2010).

[4] B. Bulka, B. Kramer, and A. MacKinnon, Z. Phys. B **60**, 13 (1985); **66**, 21 (1987); B. Kramer and A. MacKinnon, Rep. Prog. Phys. **56**, 1469 (1993).

[5] P. A. Lee and T. V. Ramakrishnan, Rev. Mod. Phys. **57**, 287 (1985).

[6] P. Soven, Phys. Rev. **156**, 809 (1967).

[7] B. Velický, S. Kirkpatrick, and H. Ehrenreich, Phys. Rev. **175**, 747 (1968); S. Kirkpatrick, B. Velický, and H. Ehrenreich, Phys. Rev. B **1**, 3250 (1970).

[8] M. H. Hettler, M. Mukherjee, M. Jarrell, and H. R. Krishnamurthy, Phys. Rev. B **61**, 12739 (2000).

[9] M. Jarrell and H. R. Krishnamurthy, Phys. Rev. B **63**, 125102 (2001); M. Jarrell, Th. Maier, C. Huscroft, and S. Moukouri, *ibid.* **64**, 195130 (2001).
[10] M. Tsukada, J. Phys. Soc. Jpn. **26**, 684 (1969).
[11] D. J. Thouless, Phys. Rep. **13**, 93 (1974).
[12] M. Janssen, Phys. Rep. **295**, 1 (1998).
[13] K. Byczuk, W. Hofstetter, and D. Vollhardt, Int. J. Mod. Phys. B **24**, 1727 (2010).
[14] *Log-Normal Distribution—Theory and Applications*, edited by E. Crow and K. Shimizu (Marcel Dekker, New York, 1988).
[15] B. Derrida, Phys. Rep. **103**, 29 (1984).
[16] V. Dobrosavljević, A. A. Pastor, and B. K. Nikolić, Eur. Phys. Lett. **62**, 76 (2003).
[17] K. Slevin and T. Ohtsuki, Phys. Rev. Lett. **82**, 382 (1999).
[18] K. Slevin and T. Ohtsuki, Phys. Rev. B **63**, 045108 (2001); New J. Phys. **16**, 015012 (2014); Phys. Rev. Lett. **78**, 4083 (1997).
[19] F. Evers and A. D. Mirlin, Rev. Mod. Phys. **80**, 1355 (2008).
[20] A. Rodriguez, L. J. Vasquez, K. Slevin, and R. A. Römer, Phys. Rev. B **84**, 134209 (2011).
[21] A. Rodriguez, L. J. Vasquez, K. Slevin, and R. A. Römer, Phys. Rev. Lett. **105**, 046403 (2010); **102**, 106406 (2009); Phys. Rev. B **78**, 195107 (2008); L. J. Vasquez A. Rodriguez, and R. A. Römer, *ibid.* **78**, 195106 (2008).
[22] G. Schubert, A. Weibe, G. Wellin, and H. Fehske, *HPC in Science and Engineering, Garching, 2004* (Springer, New York, 2005).
[23] D. Semmler, K. Byczuk, and W. Hofstetter, Phys. Rev. B **81**, 115111 (2010).
[24] C. E. Ekuma, H. Terletska, Z. Y. Meng, J. Moreno, M. Jarrell, S. Mahmoudian, and V. Dobrosavljević, arXiv:1306.5712.
[25] A. Gonis, *Green Functions for Ordered and Disordered Systems* (North-Holland, Amsterdam, 1992).
[26] See Supplemental Material at http://link.aps.org/supplemental/10.1103/PhysRevB.89.081107 for the description of how the various clusters used in our simulation are generated, how self-averaging is avoided, how the poles that emerge at criticality are handled, that $\mathrm{Im}\,\Gamma_{typ}(\omega)$ exhibits similar behavior as a function of disorder strength W. I.e., the typical hybridization rate between the impurity/cluster and the host also vanishes at the transition just as the TDOS, and the systematic approach of the critical disorder strength to the numerical value of 2.1 as the size of the cluster is increased.
[27] Y. Song, W. A. Atkinson, and R. Wortis, Phys. Rev. B **76**, 045105 (2007).
[28] The scaling of the order parameter exponent [20, 21] is $\beta = (\alpha_0 - d)\nu$, where ν is the correlation length exponent and α_0 is the zero moment of the multifractal singularity strength. The most recent estimates as reported in Ref. [20] are $\alpha_0 = 4.048$, $\nu = 1.59$, and $\beta = 1.67$.
[29] D. Vollhardt and P. Wölfle, Phys. Rev. Lett. **48**, 699 (1982); Int. J. Mod. Phys. B **24**, 1526 (2010); *Electronic Phase Transitions* (Elsevier, New York, 1992).
[30] A. Georges, G. Kotliar, W. Krauth, and M. J. Rozenberg, Rev. Mod. Phys. **68**, 13 (1996).
[31] S. Ghosh, D. A. Biava, W. A. Shelton, and D. D. Johnson, Phys. Rev. B **73**, 085106 (2006); D. A. Biava, S. Ghosh, D. D. Johnson, W. A. Shelton, and A. V. Smirnov, *ibid.* **72**, 113105 (2005).
[32] G. Schubert, J. Schleede, K. Byczuk, H. Fehske, and D. Vollhardt, Phys. Rev. B **81**, 155106 (2010).
[33] D. D. Johnson, D. M. Nicholson, F. J. Pinski, B. L. Györffy, and G. M. Stocks, Phys. Rev. B **41**, 9701 (1990).